GEOPHYSICS, VOL. 43, NO. 3 (APRIL 1978); P. 588–609, 30 FIGS.

MINERAL DISCRIMINATION AND REMOVAL OF INDUCTIVE COUPLING WITH MULTIFREQUENCY IP

W. H. PELTON*, S. H. WARD‡, P. G. HALLOF*,
W. R. SILL‡, AND P. H. NELSON§

In-situ complex resistivity measurements over the frequency range 10^{-2} to 10^{+5} Hz have been made on 26 North American massive sulfide, graphite, magnetite, pyrrhotite, and porphyry copper deposits. The results reveal significant differences between the spectral responses of massive sulfides and graphite and present encouragement for their differentiation in the field. There are also differences between the spectra of magnetite and nickeliferrous pyrrhotite mineralization, which may prove useful in attempting to distinguish between these two common IP sources in nickel sulfide exploration. Lastly, there are differences in the spectra typically arising from the economic mineralization and the barren pyrite halo in porphyry copper systems. It appears that all these differences arise mainly from mineral texture, since laboratory studies of different specific mineral-electrolyte interfaces show relatively small variations.

All of the in-situ spectra may be described by one or two simple Cole-Cole relaxation models. Since the frequency dependence of these models is typically only about 0.25, and the frequency dependence of inductive electromagnetic coupling is near 1.0, it is possible to recognize and to remove automatically the effects of inductive coupling from IP spectra.

The spectral response of small deposits or of deeply buried deposits varies from that of the homogeneous earth response, but these variations may be readily determined from the same "dilution factor" $B_2 = (\partial \ln \rho_a)/(\partial \ln \rho_2)$ currently used to calculate apparent IP effects.

INTRODUCTION

During the last two decades, conventional induced polarization and resistivity measurements have proven extremely useful in the discovery of many new mineral deposits. Along with this record of success, however, have been countless failures.

In Precambrian areas such as the Canadian, Australian, Scandinavian and, more recently, the Brazilian shield, a principal frustration with electrical prospecting methods has been the inability to distinguish between volcanogenic massive sulfide mineralization and graphitic schist. These two mineral occurrences have similar conductivities and produce approximately the same magnitude of induced polarization response. Gravity methods have been somewhat useful in distinguishing between the two, but are expensive and not particularly reliable in areas of deeper overburden, varying bedrock topography, or varying host rock density. As a result, exploration in areas containing abundant graphite has been extremely difficult and expensive, to a degree that many of these areas are left virtually unexplored. And yet, some of the largest known massive sulfide deposits in the world occur in graphitic areas and even along graphite horizons: the Kidd Creek deposit near Timmins, Ontario, the Anvil deposit in the Yukon, and the Mt. Isa deposit in Australia are prime examples.

A second major exploration difficulty in Precambrian terranes arises in the search for nickel sulfides.

Manuscript received by the Editor February 1, 1977; revised manuscript received August 29, 1977.
*Phoenix Geophysics Ltd., Willowdale, Ont., M2J 1R6 Canada.
‡Department of Geology and Geophysics, University of Utah, Salt Lake City, UT 84112.
§Lawrence Berkeley Laboratory, University of California, Berkeley, CA 94720.

The sulfides are usually found in ultrabasic environments associated with pyrrhotite, and consequently produce a resistivity low, a polarizability high, and a magnetic high. Unfortunately, horizons of increased magnetite concentration within the ultrabasics produce similar response and it is again difficult to distinguish between the two using conventional induced polarization and resistivity equipment.

Comparable difficulties exist in applying the IP method to porphyry copper exploration. The total porphyry copper system is usually readily detectable with IP, but in a majority of cases most of the response will be due to uneconomic pyrite mineralization. Some success has been achieved by applying geologic constraints and using IP as essentially a mapping tool (Pelton and Smith, 1976), but the location of economic mineralization within porphyry systems still remains a major problem.

In addition to attempting to differentiate between response caused by the barren pyrite halo and response caused by economic copper mineralization, there is an even more fundamental difficulty in the use of IP methods in porphyry copper exploration: most of the remaining undiscovered porphyry deposits in the southwestern U.S. lie deep beneath conductive alluvial sediments. As a result there is great difficulty in differentiating between IP response due to mineralization and that due to inductive electromagnetic coupling. An approximate scheme designed to remove inductive coupling has been suggested by Hallof (1974) and a computer interactive scheme has been suggested by Wynn and Zonge (1975). However, the use of these methods has been limited.

Several years ago, at the start of our research into the application of multifrequency IP or complex resistivity methods, we realized that there was basically very little information available on the IP response of various types of mineralization over a large frequency range. The questions we raised were fundamental: (1) what are the typical IP spectra, (2) are there mathematical models which fit these spectra, (3) is there a common model, (4) do any of the model parameters show significant variation with grain size, concentration, or mineral type, (5) what are the differences in IP spectra over a finite-sized mineral deposit as opposed to spectra over a homogeneous earth, and (6) are there any inherent differences between the spectra arising from mineralization and those arising from inductive coupling. In this paper we will attempt to address these fundamental questions, and in the process perhaps demonstrate how spectral IP measurements might be usefully applied to practical mining exploration problems.

COLE-COLE MODEL

An exceedingly simple relaxation model which has

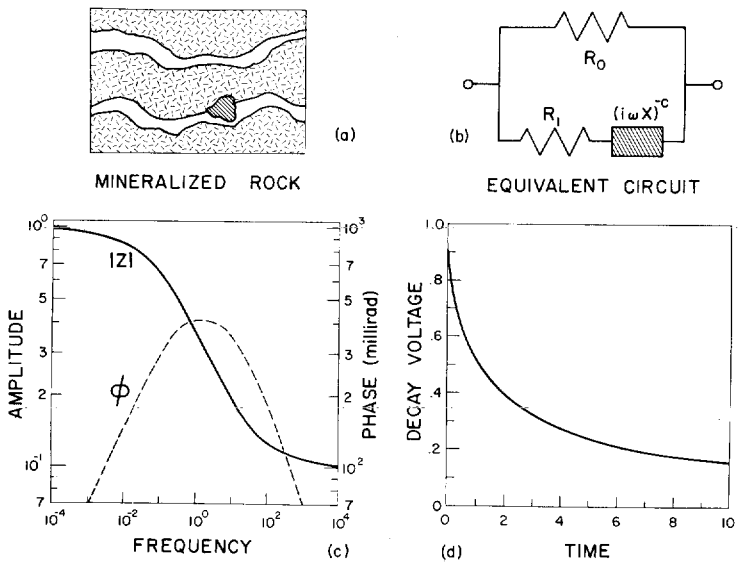

FIG. 1. (a) A small section of a mineralized rock which has both blocked and unblocked pore passages. (b) An equivalent circuit for the mineralized rock. (c) Typical frequency domain response for the equivalent circuit. (d) Time domain response corresponding to the frequency domain response plotted in (c).

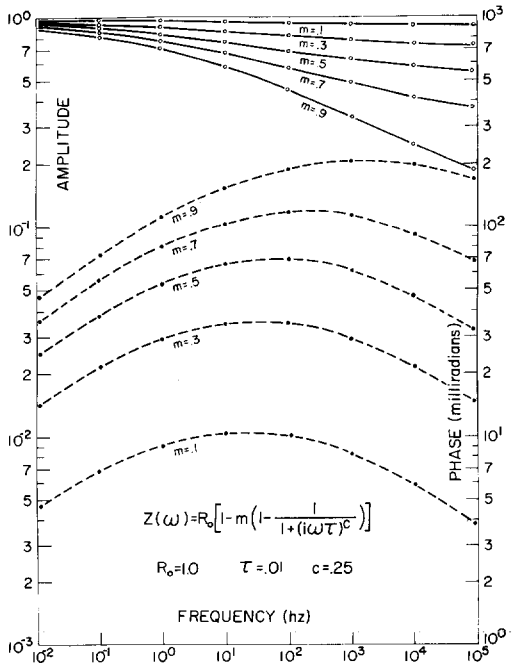

FIG. 2. Amplitude and phase curves for a Cole-Cole relaxation model with $R_0 = 1.0$, $\tau = .01$, $c = .25$, and m varying from 0.1 to 0.9.

been found to fit a variety of laboratory complex resistivity results (Madden and Cantwell, 1967; Pelton et al, 1972) was originally proposed by Cole and Cole (1941) to predict complex dielectric behavior. The circuit of Figure 1b is a resistive network which exhibits a Cole-Cole relaxation. Other equivalent circuits can be envisioned which also have the same response, but this one provides a convenient analogy to one view of the pore geometry in a mineralized rock which is shown in Figure 1a. In the circuit, the complex impedance, $(i\omega X)^{-c}$ simulates the metallic-ionic interface. The resistance R_0 simulates unblocked pore paths by allowing parallel conduction through a purely resistive element, and the resistance R_1 simulates the resistance of the solution in the blocked pore passages. A word of caution is in order, in that this view of a small section of mineralized rock is admittedly too simple; the true conduction paths are certainly more complicated. However, this simple model and equivalent circuit allow us to derive virtually all the essential features of IP spectra observed in the laboratory and the field.

The general behavior of the equivalent circuit with frequency is given in Figure 1c. It is obvious that at very low frequency only the purely resistive path can carry current. As a result, the amplitude of the impedance asymtotes to R_0. At very high frequency, the complex impedance becomes negligible with respect to R_1, so that the total impedance is just R_1 in parallel with R_0. Between these two asymptotes there is a dispersive region where the amplitude of the impedance slowly decreases, and the phase angle reaches a maximum. On a double logarithmic plot, the phase is entirely symmetric about this maximum: at low frequencies the phase has a slope of $+c$, and at high frequencies it has a slope of $-c$.

Since the impedance of the circuit is not zero at infinitely high frequency, there must be a discontinuity in the time-domain response of the circuit. If we adopt the definition for chargeability m proposed by Seigel (1959) as being the ratio of voltage immediately after, to the voltage immediately before cessation of an infinitely long charging current, we may write the expression for the impedance of the equivalent circuit as

$$Z(\omega) = R_0\left[1 - m\left(1 - \frac{1}{1 + (i\omega\tau)^c}\right)\right], \quad (1)$$

where

$$m = \frac{1}{1 + \dfrac{R_1}{R_0}}, \quad (2)$$

and

$$\tau = X\left(\frac{R_0}{m}\right)^{1/c} \quad (3)$$

The second parameter τ, or "time constant" as we choose to call it, has the units of seconds and determines the length of time required for the decay in the time domain. If the frequency dependence c is equal to 1.0, the time-domain decay has the familiar negative exponential form,

$$V(t) = m\frac{R_0}{I_0}e^{-t/\tau}, \quad (4)$$

where I_0 is the magnitude of the infinitely long charging current.

Laboratory studies of IP (Madden and Cantwell, 1967; Pelton et al, 1972) have suggested, however, that the frequency dependence is not equal to 1.0, but is typically in the range 0.1 to 0.6. As a result, the IP decay is slower than exponential, as illustrated by Figure 1d, and takes the general form,

$$V(t) = m\frac{R_0}{I_0}\sum_{n=0}^{\infty}\frac{(-1)^n\left(\dfrac{t}{\tau}\right)^{nc}}{\Gamma(nc+1)}, \quad (5)$$

where $\Gamma(x)$ is the gamma function. Since $\Gamma(x + 1) = x!$ when x is an integer, (5) reduces to (4) when $c = 1.0$.

We have attempted to demonstrate in this section how a very simple view of a mineralized rock results in a relaxation model containing only four parameters, which predicts IP behavior in both the frequency domain and the time domain. The four parameters are the dc resistivity R_0, the chargeability m, the time constant τ, and the frequency dependence c. In Figure 2, we show the amplitude and phase curves for $R_0 = 1.0$, $\tau = .01$, $c = 0.25$ and $m = 0.1$ to 0.9. It is evident that the main effect of increasing the chargeability is to increase the polarizability or phase angle. The effect of changing the frequency dependence c is demonstrated by Figure 3, where the same curves are shown for a value $c = 0.5$. Since the dispersion takes place in a frequency interval only half as wide, the slope of the amplitude curves is steeper and the phase angle curves are more peaked.

We have not shown separate graphs which illustrate the effects of increasing τ and increasing R_0 since these changes are trivial in concept. For example, if τ is increased by one decade, both amplitude and phase curves are shifted one decade horizontally to the left along the frequency axis. If R_0 is increased by one decade, the amplitude curves are shifted one decade vertically along the resistivity axis. The phase angle curves depend only on m, τ, and c; thus they remain fixed.

Although the Cole-Cole model is extremely simple, it provides a quantitative description of IP spectra. The variation of only one parameter, the time constant τ, is able to provide the effects noted by earlier qualitative characterizations such as concave-up and concave-down spectra (Fraser et al, 1964) and type A, B, and C spectra (Zonge and Wynn, 1975).

We hope that the brief, utilitarian treatment of the Cole-Cole model given here might suffice for this paper since a second paper has been prepared which more fully explores the Cole-Cole model and alternative models for complex resistivity and dielectric behavior. However, we would like to clear up several points which, in review, appear confusing. The relaxation model proposed by Cole and Cole in 1941, was originally applied only to complex permittivity, whereas in this paper we have used the same mathematical form to describe complex resistivity. As shown previously in this section, the form can be derived quite naturally by simple analysis of a small section of rock where a metallic particle is blocking one of the pore passages. For this ideal case, the dominant physical mechanism controlling the passage

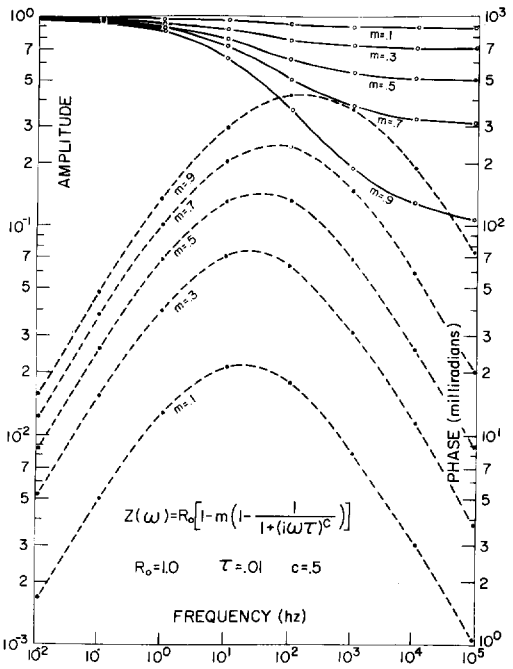

FIG. 3. Amplitude and phase curves for a Cole-Cole relaxation model with $R = 1.0$, $c = 0.5$, and m varying from 0.1 to 0.9.

of current through the blocked passage is diffusion, and the frequency dependence of the Cole-Cole model is 0.5. However, in a natural rock there are many different pore passages which are blocked by minerals having a wide range of grain size. The result is a broader dispersion and consequently a smaller frequency dependence.

An additional source of possible confusion is the expression we have derived for the time constant given in (3). Our tendency throughout this paper is to use R_0, m, τ, and c as the fundamental parameters describing IP spectra. There are two reasons for this: first, the expressions for the Cole-Cole model in the frequency domain (1) and in the time domain (5) appear in their simplest possible form; and second, the four parameters form the basis which presently appears most useful and convenient for mineral discrimination. This is not the only basis; the four parameters of the equivalent circuit (R_0, R_1, X, and c) offer a logical alternative. Indeed, they may seem to be a better alternative since no parameter is coupled to any other, whereas (3) shows the time constant expressed in terms of all three of the other parameters forming the basis. The weakness in this line of reasoning is that the simple equivalent circuit shown in

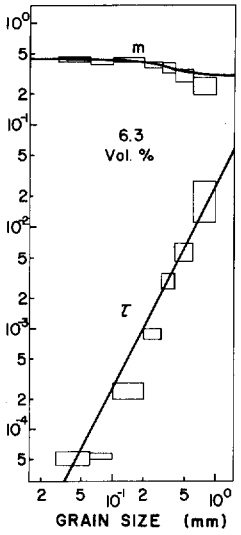

FIG. 4. Variation in chargeability and time constant as a function of grain size. The plots were obtained from inversion of results reported by Grisseman (1971) for artificial rocks composed of cement, quartz sand, and pyrite.

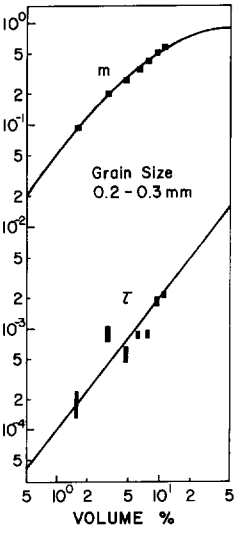

FIG. 5. Variation in chargeability and time constant as a function of sulfide concentration. The plots were obtained from inversion of results reported by Grisseman (1971) for artificial rocks composed of cement, quartz sand, and pyrite.

Figure 1b is an extremely idealized representation of a mineralized rock, and thus the equivalent circuit parameters have really no more inherent importance than the four parameters used to describe the spectra in (1). In spite of this weakness, the equivalent circuit and equation (3) can be used to provide some indication of what the IP spectra should be like when the resistivity of the rock is very high; namely, the time constant of the relaxation should be very long. This has indeed been observed in measurements of highly resistive artificial rocks.

A final point, which we would like to clarify, is our omission of dielectric conduction in the mathematical forms we have adopted for complex resistivity. This was only possible because the resistivities of the mineralized rocks which we measured were low enough that dielectric conduction played a negligible role in the total current conduction through the rock. If the resistivities had been higher or if we had made measurements at higher frequency, it would be necessary to include the contribution of dielectric conduction in our mathematical expression for complex resistivity. Again, this subject has been treated much more fully in a second paper.

EFFECTS OF CONCENTRATION AND GRAIN SIZE

Before attempting to discern what differences in IP spectra might arise between different types of mineralization, it was decided to investigate, briefly, changes occuring with grain size and concentration.

A study of pyrite in artificial rocks has been carried out by Grisseman (1971). Although there was some difficulty with the data in that the real and imaginary results do not precisely obey the causality relations, we managed to fit the real conductivity spectra to the Cole-Cole model very accurately using a ridge regression inversion program (Pelton et al, 1974).

It was evident from the original data that changing the concentration of the pyrite and the grain size had relatively minor effect on the dc resistivity R_0. We also found from the inversion that there was relatively minor change in the frequency dependence c; it was usually in the range 0.4 to 0.6. The two remaining parameters m and τ, however, showed pronounced variation with both grain size and concentration as illustrated in Figures 4 and 5. We extrapolated the trends observed in these figures in order to create the contours shown in Figure 6. Although the data are very limited in that they apply only to artificial rocks composed of cement, quartz-sand, and pyrite, the results indicate two main trends, illustrated as arrows on Figure 6. The effect of increasing concentration is to increase both the chargeability and the time constant, whereas the effect of increasing grain size is to

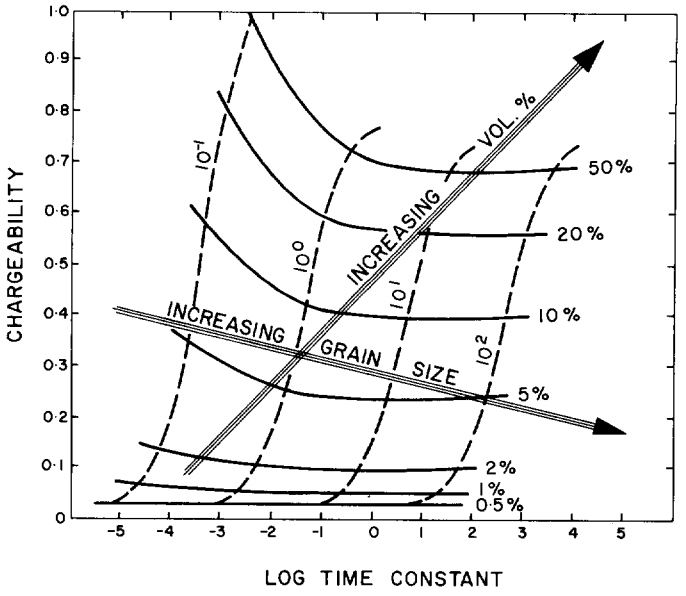

FIG. 6. The trends observed in Figures 4 and 5 have been extrapolated to provide contours of sulfide concentration (volume percent) and grain size (mm) in chargeability-time constant space. The arrows are approximately perpendicular to the contours, and indicate increasing sulfide concentrations and increasing grain size.

increase the time constant but to decrease the chargeability. We will return to these major trends in our interpretation of in-situ IP spectra over porphyry copper deposits.

IN-SITU FIELD MEASUREMENTS

Although laboratory measurements on natural rocks were useful in suggesting the general form of the IP response, and studies of artificial rocks gave some idea of the changes in IP spectra which might be caused by grain size or concentration, these studies have limited application in determining the true bulk IP response of mineral deposits encountered in electrical prospecting. The main problem with laboratory measurements on drill cores is that the sample size is much too small to duplicate the conduction currents through fractures and veins which occur in the field. The problem with artificial rocks is that the pore structure created in concrete samples probably bears little resemblance to that of natural rocks.

Thus, in order to determine accurately the IP response of naturally occurring mineral deposits, we decided to make in-situ measurements. In-situ spectral IP measurements have been made previously (Hallof, 1965; Van Voorhis et al, 1973; Zonge and Wynn, 1975), but they cover a relatively limited frequency range. We made measurements over seven decades of frequency from 10^{-2} Hz to 10^{+5} Hz in order to determine (1) if the Cole-Cole model was an accurate description of natural IP behavior, (2) if there were pronounced differences in spectra between different types of mineral occurrences, and (3) if inductive coupling was inherently different from natural IP behavior.

To cover this broad frequency range we used two sets of equipment. For the low frequency range from 10^{-2} Hz to 5.0 Hz we used a digital tape recorder system supplied by Kennecott Exploration Services and described by Van Voorhis et al (1973). For the higher frequencies, from 5.0 Hz to 60 kHz, we used a Hewlett Packard 203A oscillator for the transmitter and a Princeton Applied Research lock-in amplifier for the receiver.

To avoid inductive coupling at the highest frequencies, we used a dipole-dipole array with an extremely small electrode separation—typically 1 m. Since the inductive coupling depends on the frequency times the square of the electrode interval, reducing the electrode interval by a factor of 100 below typical field values permitted us to use frequencies higher by a factor of 10,000.

As a result of the short electrode spacing used to avoid inductive coupling, we were very restricted in the depth of penetration of our measurements. We therefore decided to make all of our measurements on mineralization exposed in open pit mines or on

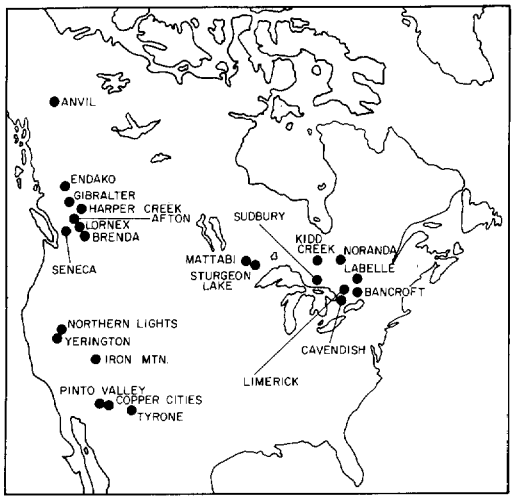

FIG. 7. Locations of mineral occurrences where in-situ multi-frequency IP measurements were made.

fresh outcrop. The different mineral localities which we visited in the summers of 1974 and 1975 are illustrated in Figure 7. In several of the localities, there were two distinctly different mineral occurrences such as graphite and massive sulfides. We thus made a total of more than 90 measurements on 26 different mineral occurrences. In addition to making the in-situ measurements on several tons of mineralization, we gathered bulk samples for chemical analysis, petrographic studies, and further laboratory measurements.

Porphyry copper deposits

The first in-situ data we will discuss are results obtained over porphyry copper mineralization. Earlier studies by Van Voorhis et al (1973) had suggested that the phase angle was almost constant, as a function of frequency, for porphyry mineralization. Our studies over a larger frequency range indicated that while the variation of the phase angle with frequency is very gentle for some deposits, the phase angle nonetheless does vary, and the variation can be described accurately by one or two Cole-Cole relaxations.

Figure 8 shows phase angle results obtained from the Lornex deposit in British Columbia. The mineralization is typical of several other deposits in the Highland Valley area of B.C. Since the total concentration of sulfide minerals is low and since the sulfides commonly occur as discrete disseminated grains, we call the deposit a "dry" porphyry (Pelton and Smith, 1976). We have found that for this type of deposit, the phase angle is usually an increasing function of frequency until it reaches a maximum somewhere above 10 to 100 Hz. This behavior corresponds to a Cole-Cole relaxation model with a small time constant.

Another example of results obtained over a dry porphyry is shown in Figure 9. The data are from the Copper Cities deposit in Arizona. In addition to the main IP dispersion which results in a phase angle maximum near 100 Hz, we have another dispersion occurring at much higher frequencies. This high-frequency dispersion is possibly due to membrane polarization effects (Katsube, 1976). The calculated effects for inductive coupling suggest that as long as the resistivity is greater than about 6 Ω-m for a 1 m electrode spacing and a frequency of 60 kHz, the phase angle response is less than 10 mrad (Millet, 1967). The resistivity we obtained for this measurement on the Copper Cities deposit was 100 Ω-m, yet the phase angle at 60 kHz was 170 mrad. While this high-frequency response is perhaps intriguing, it is not

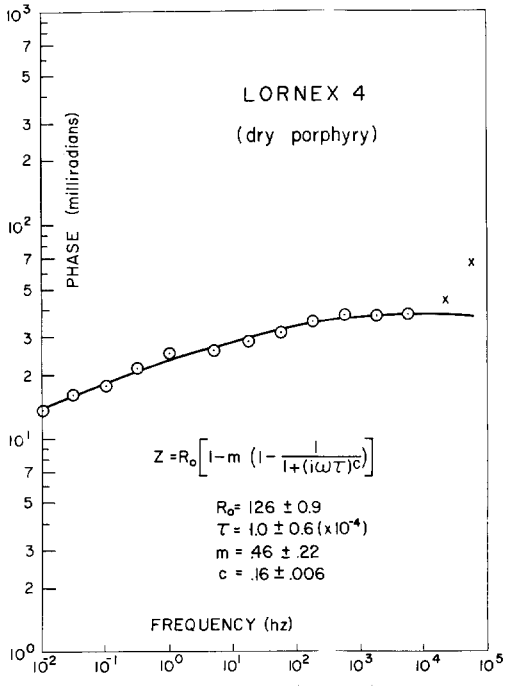

FIG. 8. Phase angle spectra from the Lornex porphyry copper deposit in Highland Valley region of British Columbia. Dipole-dipole array: $n = 1$, $x = 1$ m. The circles represent the observed data, the solid line represents the best-fitting theoretical curve, and the crosses represent possibly noisy data which were not used in the inversion.

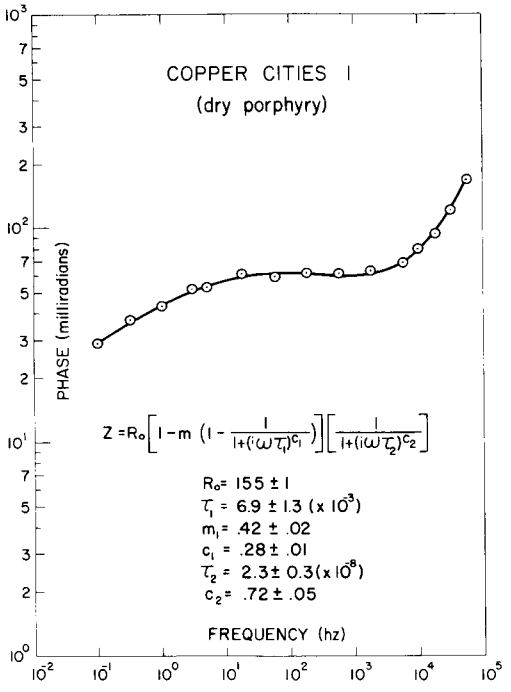

FIG. 9. Phase angle spectra from the Copper Cities porphyry copper deposit in the Globe-Miami district of Arizona. Dipole-dipole array, $n = 1$, $x = 1$ m.

particularly useful since it occurs at frequencies much higher than would normally be used in the field and is also seen in unmineralized rocks. We thus tend to fit two dispersions to the data, as we have done in Figure 9, but restrict our attention to the parameters describing the main IP dispersion occurring at the lower frequencies.

Figure 10 shows data from the Tyrone porphyry copper deposit in New Mexico. We use these data to illustrate response from a "wet" porphyry. The sulfide mineral concentration was high (17 percent), and the minerals were typically distributed as veins and veinlets rather than as discrete disseminations. Although the curve was fitted to two Cole-Cole relaxations, as were the data from Copper Cities, we note that the phase angle maximum occurs at much lower frequencies and that the time constant for the main IP dispersion is much larger.

Data from another wet porphyry, the Gibraltar deposit in British Columbia, are shown in Figure 11. Again we note that the time constant is much larger than those obtained over the dry porphyries, and that the chargeability is also typically larger, resulting in phase angles of greater magnitude.

In Figure 12, we have plotted all the results obtained over porphyry mineralization in chargeability —time constant space. The chargeabilities and time constants associated with the known wet porphyries such as Gibraltar and Tyrone are all distinctly larger than those associated with the typically dry porphyries such as Lornex and Brenda. Other deposits such as Yerington yielded a variety of mineral occurrences ranging from low concentrations of sulfides occurring as discrete disseminations to 10 percent chalcopyrite distributed as veinlets. Thus the parameters sometimes covered a broad range of values for a single deposit.

Two of the porphyries were unusual in that the most important economic minerals were molybdenum (Endako) and native copper (Afton). We found that the disseminated native copper at Afton produced data very similar to that of disseminated chalcopyrite at Lornex and Brenda. The results from Endako were more intriguing. Measurements over massive 1 ft veins of molybdenite failed to produce a significant resistivity low or polarizability high. Further laboratory studies revealed resistivities ranging from 10^3 to 10^5 Ω-m for small samples containing 50 percent

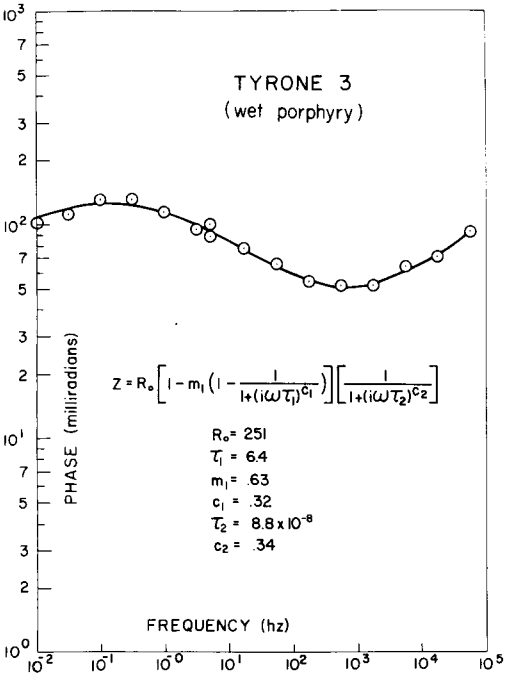

FIG. 10. Phase angle spectra from the Tyrone porphyry copper deposit near Silver City, New Mexico. Dipole-dipole array, $n = 1$, $x = 1$ m.

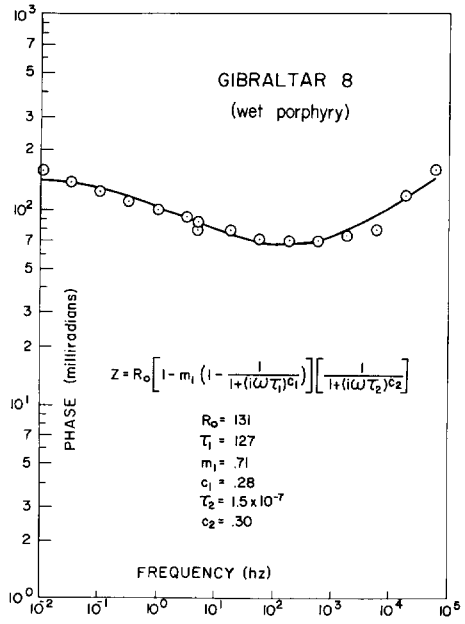

FIG. 11. Phase angle spectra from the Gibraltar porphyry copper deposit near Williams Lake, B.C. Dipole-dipole array, $n = 1$, $x = 1$ m.

molybdenite. These high resistivities explain the very low measured IP effects. Due to the high resistivity of the mineralization, the conductivity at very high frequency is not appreciably greater than the conductivity at dc. This results in a low chargeability and accounts for the observed low phase angle response (10 to 15 mrad).

Using the values of sulfide concentration obtained from nearby drill holes and from our bulk samples, we constructed the plot shown in Figure 13. Superimposed on the plot is the arrow showing the trend for increasing concentration derived from our analysis of Grisseman's data on artificial rocks. The trend is the same for both sets of data; increasing concentration results in increasing chargeability and increasing time constant.

The other main trend observed from the analysis of artificial rock data is shown in Figure 14, again along with our in-situ results on porphyry mineralization. Since a great range of grain sizes occurred for each in-situ measurement, we attempted to place the data into only two broad groups. The closed symbols correspond to mineralization occurring as discrete disseminations with nominally small grain size, whereas the open symbols correspond to mineralization typically occurring in veinlets, and thus larger effective grain size. Again the in-situ results

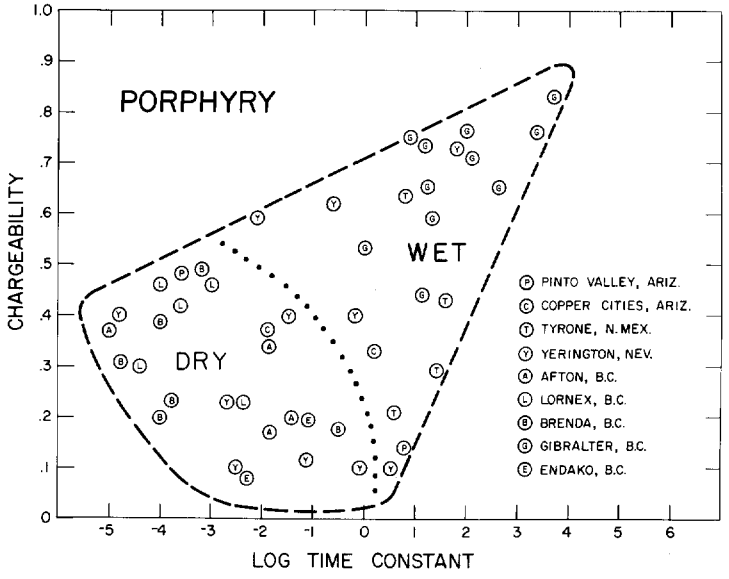

FIG. 12. Summary of the spectral IP data obtained from porphyry deposits plotted in chargeability-time constant space. The dotted line roughly divides the measurement sites into two groups according to the type of mineralization observed at each site. "Dry" indicates that the total concentration of sulfide minerals is low and that the sulfides commonly occur as discrete disseminated grains. "Wet" indicates that the total concentration of sulfide minerals is high and that the sulfides typically occur as veins and veinlets.

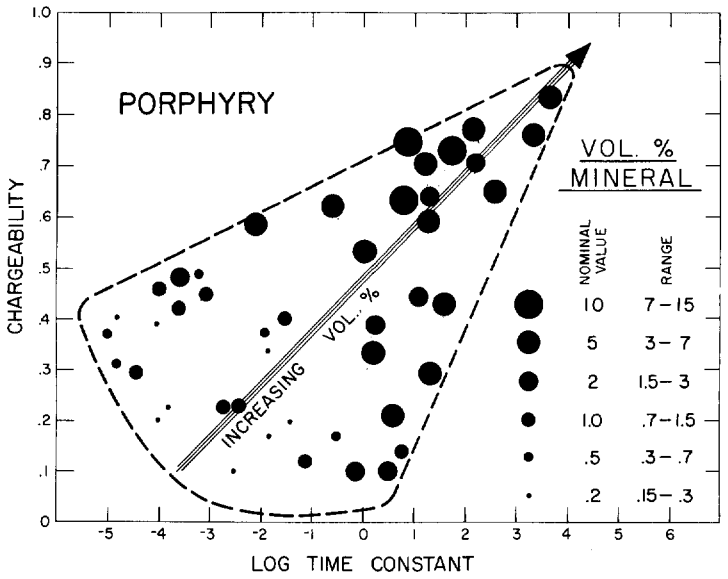

FIG. 13. Data from porphyry deposits plotted in chargeability-time constant space. The larger dots indicate high sulfide concentration. Superimposed on the plot is the arrow from Figure 6 which indicates the trend due to increasing volume percent sulfides in artificial rocks.

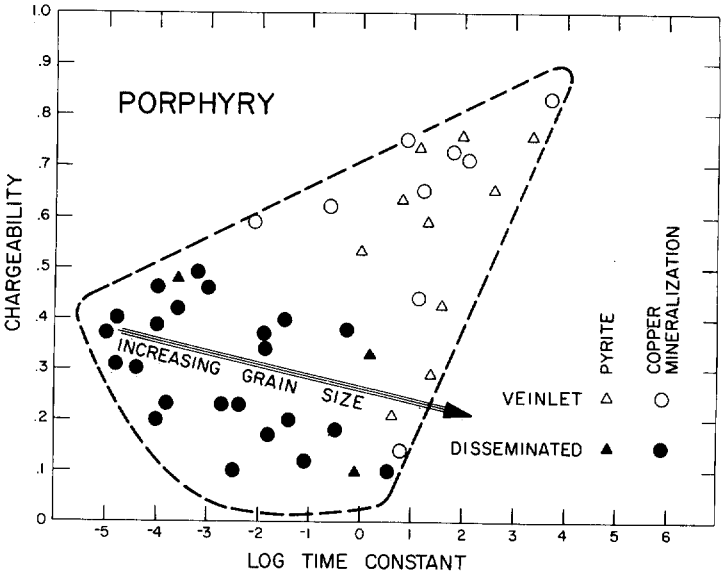

FIG. 14. Data from porphyry deposits plotted in chargeability-time constant space. There is a grouping of veinlet mineralization (open symbols) versus discretely disseminated mineralization (closed symbols) but there is no distinct grouping of pyrite mineralization (triangles) versus copper mineralization (circles). Superimposed on the plot is the arrow from Figure 6 which indicates the trend due to increasing grain size in artificial rocks.

basically confirm the trend observed from the artificial rock studies: as the grain size increases, the time constant increases, but the chargeability decreases slightly.

We have used circles and triangles in Figure 14 to try to illustrate another point of major importance. There *is* a grouping of veinlet versus disseminated mineralization in chargeability-time constant space, but there is *no* such grouping of pyrite (triangles) versus copper mineralization (circles). We found, for example, that veinlet chalcopyrite mineralization at Yerington gave very similar response to veinlet pyrite mineralization at Gibraltar. Thus it seems that the main differences in spectra arise from mineral habit or texture and not from mineral composition. Spectral IP measurements can still be useful in locating economic mineralization within porphyry systems; however, since chalcopyrite often occurs as discrete disseminations near the core of the porphyry whereas pyrite typically occurs as veinlets

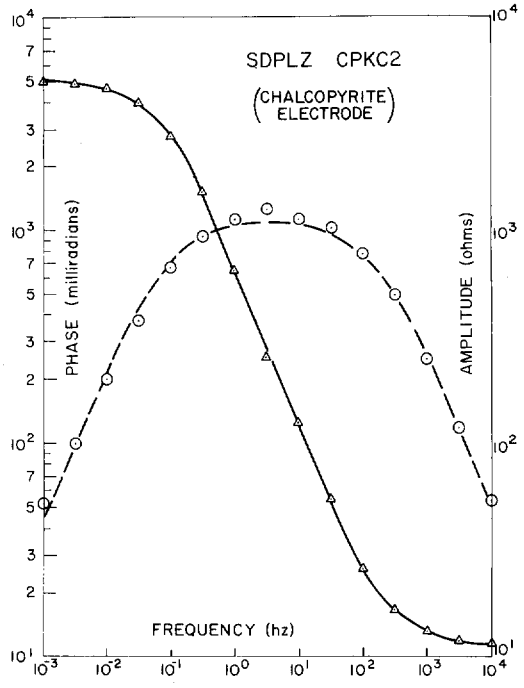

FIG. 15. Amplitude and phase angle spectra obtained by passing current through two chalcopyrite electrodes separated by 5 mm of 0.1 n NaCl solution. The area of each electrode was approximately 4 cm^2 and the electrode surfaces were polished to 20 microns. To simulate the effects of additional unblocked current paths and to increase the decay rate of transient effects, a 5600-Ω resistor was placed in parallel with the two electrodes.

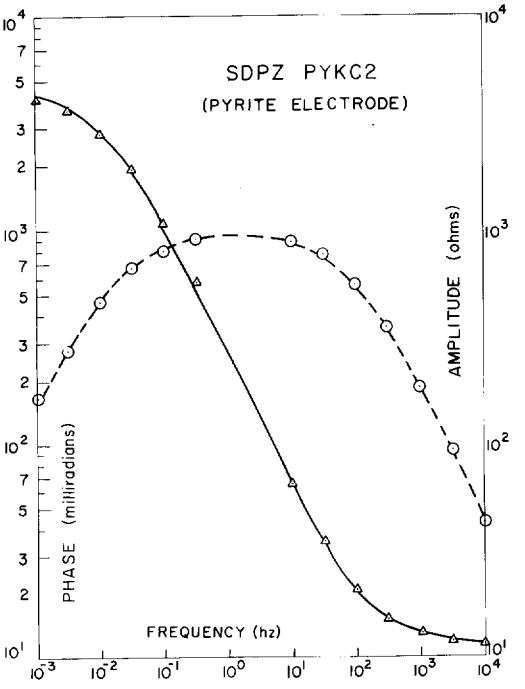

FIG. 16. Amplitude and phase angle spectra obtained by passing current through two pyrite electrodes separated by 5 mm of 0.1 N NaCl solution. The area of each electrode was approximately 4 cm^2 and the electrode surfaces were polished to 20 microns. A 5600-Ω resistor was placed in parallel with the two electrodes.

in the surrounding halo. Caution must be exercised, though, in that these textural trends are certainly not invariant.

Since our results somewhat conflict with suggestions by others that chalcopyrite and pyrite IP response were intrinsically different, we decided to carry out additional measurements in the laboratory on small mineral specimens. Figures 15 and 16 give results obtained from passing current between two chalcopyrite electrodes and two pyrite electrodes (Klein and Pelton, 1976). The spectra obtained were very similar. At the highest frequencies the amplitude of the complex resistance (solid line) asymptoted to the resistance of the solution between the electrodes (0.1 N NaCl), whereas at the lowest frequencies it asymptoted to the value of a 5.6 K shunt resistor placed in parallel. Between these two asymptotes, the complex resistance was determined by the impedance arising from the two metallic-ionic interfaces in series. Each set of data was quite accurately fitted by a single Cole-Cole relaxation model with the

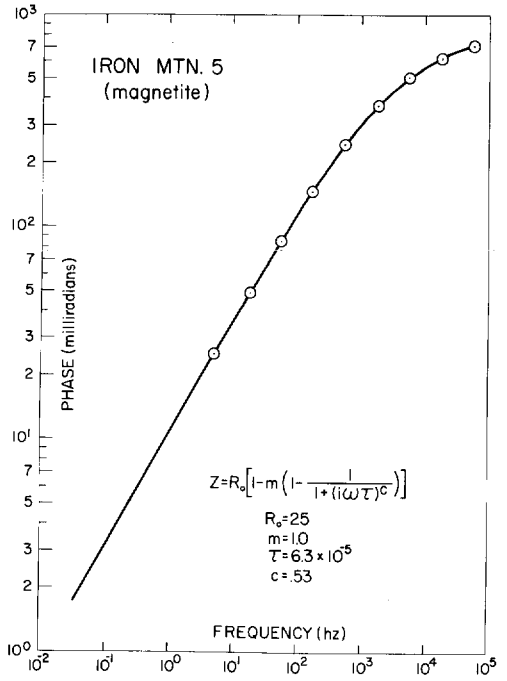

FIG. 17. Phase angle spectra from the Mountain Lion magnetite deposit at Iron Mtn. in southern Utah. The circles represent the observed data and the solid line represents the best fitting theoretical curve.

frequency-dependence c near 0.5 and the value of the complex impedance differing by less than a factor of 3.0 for the two electrode sets. These results tend to confirm that there is relatively minor difference between the inherent polarizability of pyrite and chalcopyrite, so that the observed differences in in-situ spectra over porphyry mineralization appear to be caused by mineral texture and not composition.

Magnetite and pyrrhotite deposits

Another objective in our program of in-situ measurements was to compare spectra over magnetite with that over nickeliferrous pyrrhotite mineralization. We hoped to be able, perhaps, to discriminate between these two common IP sources in nickel sulfide exploration. Figure 17 shows results obtained over very powdery magnetite mineralization exposed in an open pit mine near Iron Springs, Utah. Although the ore was 76 percent magnetite, there apparently is little electrical continuity between each of the many small mineral grains. As a result, the spectra indicate a dispersion at very high frequency and the time constant is very small.

Just the opposite textural trend was observed for pyrrhotite mineralization. At Sudbury, Ontario and at the other pyrrhotite occurrences which we visited, there was a very great tendency for the mineralization to connect together to form veinlets. When the host rock contained even less than 5 percent pyrrhotite, the resistivity of the rock was often less than 0.1 Ω-m. When we encountered resistivities this low, we were usually required to place most of our dipole-dipole array on unmineralized host rock in order to achieve voltages large enough for accurate measurement. As shown in Figure 18, the spectra which we found typical of pyrrhotite mineralization indicated a dispersion at very low frequency, and consequently a very long time constant.

The results of all our measurements on pyrrhotite and magnetite mineralization are summarized in Figure 19. In some deposits, where the magnetite mineralization was massive as opposed to powdery, the time constants were fairly large, but for most deposits the time constants obtained were considerably smaller than those from pyrrhotite. The great range in chargeability for the magnetite was a result of very large changes in concentration—from a few percent to massive.

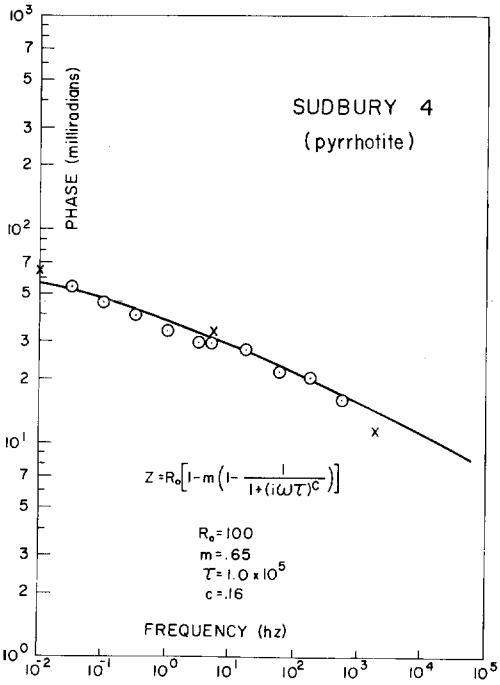

FIG. 18. Phase angle spectra from the Gertrude nickeliferrous pyrrhotite deposit near Sudbury, Ontario.

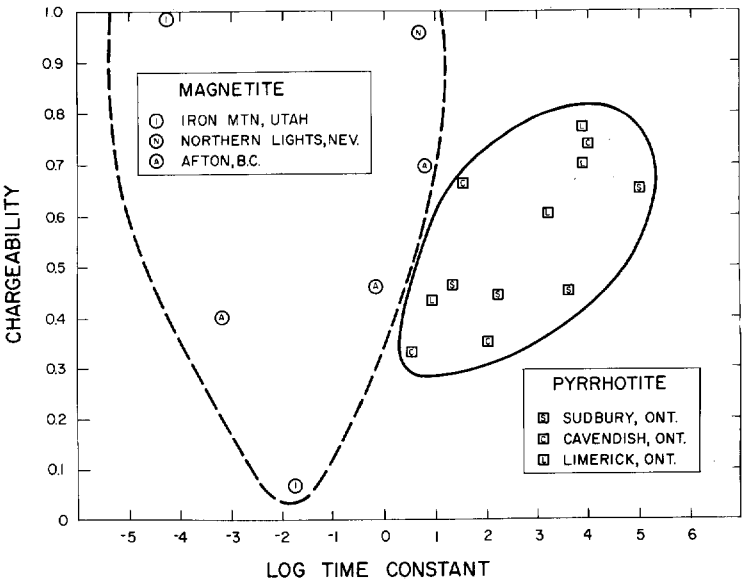

FIG. 19. Summary of the spectral IP data obtained from magnetite and pyrrhotite deposits plotted in chargeability-time constant space.

To check if there were differences in the inherent polarizability of magnetite and pyrrhotite, we duplicated the laboratory measurements described earlier for chalcopyrite and pyrite. We found that the magnetite and pyrrhotite spectra were very similar to each other and, in turn, similar to those obtained earlier for pyrite and chalcopyrite. As a result, it appears that the differences in the in-situ spectra observed for magnetite and pyrrhotite again result largely from differences in texture and not from differences in composition. Although it is perhaps somewhat circuitous to suggest discrimination based on differences in IP spectra caused by differing texture, it may turn out to be reasonably reliable and effective, as long as nickeliferrous pyrrhotite habitually occurs in veinlets and magnetite typically has poor electrical connection between individual grains.

Artificial rock studies by Sill and DeWitt (1976) suggest that if differences in electrode impedances for various minerals are present they can lead to changes in the spectra, notably shifts in the time constant of the relaxation. However, these studies also demonstrate the very strong dependence of the time constant on the length scale (i.e., grain size and texture) of the mineralization.

Graphite and massive sulfide mineralization

As we mentioned earlier, perhaps the single greatest limitation in the application of electrical prospecting methods in Precambrian terranes is the inability to discriminate between graphitic schist and volcanogenic massive sulfide mineralization. Thus, one of the more important objectives in our program of in-situ measurements was to obtain data over these two different types of mineral occurrences. Initially, we were rather pessimistic about the outcome of such measurements. One reason was the widely held belief that massive sulfides were not inherently polarizable; that IP anomalies over these deposits were predominantly caused by the single frequency-dependent interface between the host rock and the sulfides, similar to the response caused by a buried metal pipe. If this were indeed the only polarization mechanism, the spectral IP response over a massive sulfide deposit could be expected to appear very similar to the response over typically well-connected graphite mineralization.

We were thus relatively surprised when we measured our first IP spectra over the Seneca massive sulfide deposit in British Columbia, and found that the phase angle response reached a maximum near 100 Hz, similar to the response usually recorded over disseminated mineralization. Since the actual massive sulfide mineralization was covered by debris left in the trench where we made our measurements, we tentatively attributed the response to disseminated mineralization surrounding the sulfides.

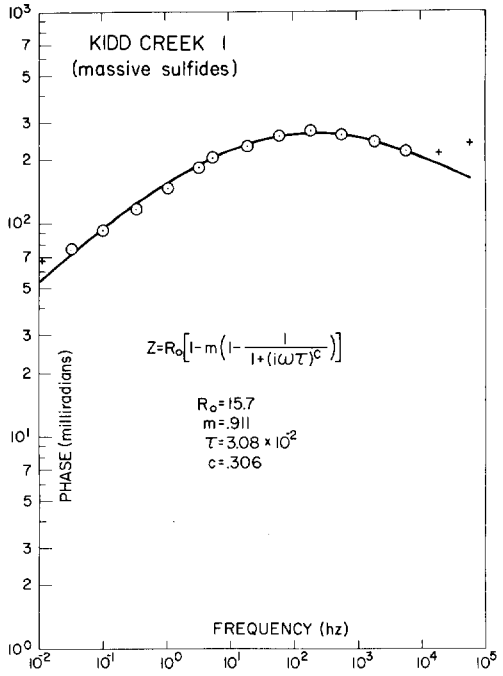

FIG. 20. Phase angle spectra from the Kidd Creek massive sulfide deposit near Timmins, Ontario. The circles represent the observed data, the solid line represents the best-fitting theoretical curve, and the crosses represent possibly noisy data which were not used in the inversion.

At our next set of measurements on the Anvil deposit in the Yukon Territory, and at the succeeding Sturgeon, Mattabi, and Kidd Creek deposits in Ontario, we had no such difficulty in getting direct access to the massive sulfide mineralization. All of the measurements were made in open pit mines on large exposed sections of mineralization on the pit floor, and all of the data showed large phase angles which peaked at high frequency. Since our 1 m dipole-dipole array was typically surrounded by 10 m of massive sulfides, it was evident that no host rock-massive sulfide interface was involved, and that no surrounding disseminated mineralization was contributing to the response.

As illustrated by the data from Kidd Creek in Figure 20, the results suggest that volcanogenic massive sulfides are inherently very polarizable, and that the spectral response is similar to that of disseminated sulfides in that the time constant is small. The main difference between the two is that the chargeability associated with the massive sulfides is much higher than that for disseminated mineralization.

In keeping with our emphasis on mineral texture as the factor primarily responsible for characterizing spectral IP response, it appears that the typical granular appearance of volcanogenic massive sulfide mineralization may perhaps hold the answer to its spectral behavior. Just as we observed very high chargeabilities and small time constants associated with massive, powdery magnetite, and attributed this response to poor electrical connection between the individual magnetic grains, we might also be led to believe that there is poor electrical connection between the grains comprising the matrix of massive sulfides: that instead of few metallic-ionic interfaces per unit volume, as in veined mineralization, there are many interfaces, corresponding to the boundaries of each individual grain.

We should mention here that where massive sulfides do not have this typical granular or "sugary" texture, the spectral IP response may be different. In one exposed massive sulfide deposit near Noranda, Quebec, we found that the resistivity was too low to permit spectral IP measurements with our equipment. The sulfides had evidently undergone extreme metamorphism and were very hard. It is possible that the original massive sulfide grains may have

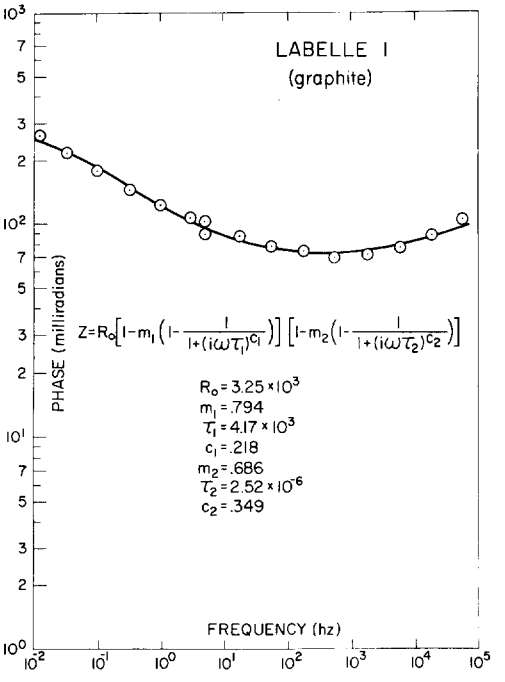

FIG. 21. Phase angle spectra from a graphite deposit near Labelle, Quebec.

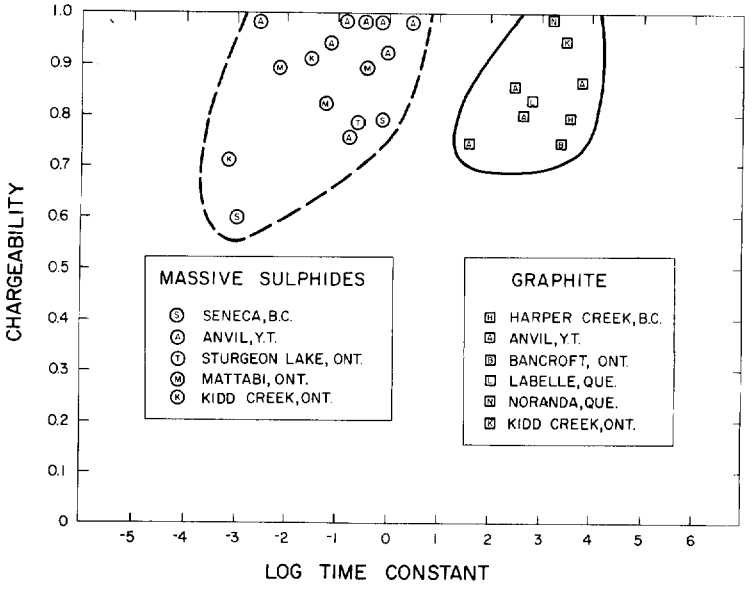

FIG. 22. Summary of the spectral IP data obtained from massive sulfide and graphite deposits plotted in chargeability-time constant space.

been fused together or that pyrrhotite may have been formed to create greater electrical connectivity.

The results we obtained over graphite mineralization were consistent with our original expectations. Graphite, like pyrrhotite, appears to be habitually well-connected: concentrations of only a few percent form continuous veins and produce generally high conductivity. It was therefore not surprising when the spectra we obtained over graphite turned out very similar to that obtained over veined pyrrhotite mineralization and veined pyrite mineralization in "wet" porphyry deposits. Spectra from graphite mineralization near Labelle, Quebec are shown in Figure 21. The high phase angle response at low frequency corresponds to high chargeability and large time constant.

Summarized in Figure 22 are all the results over graphite and massive sulfide deposits plotted in chargeability-time constant space. Although the chargeabilities determined over the two types of mineral occurrences are similar, the time constants tend to differ by three or four orders of magnitude; thus the deposits fall into two distinct groups: graphite characterization by extremely long time constants and massive sulfides by very short time constants.

In order to determine if the differences in time constant might be caused by differences in the impedance of the metallic-ionic interface, we again carried out laboratory measurements on small specimens of massive sulfides and graphite. The parameters relating to the interface impedance of graphite turned out to be very similar to those obtained earlier from studies of massive pyrite and massive chalcopyrite. Thus, we are again led to believe that the large observed differences in in-situ spectra over graphite and massive sulfides arise primarily from differences in mineral texture and not from differences in electrochemical conduction at the mineral-electrolyte interface.

Frequency dependence and resistivity

Throughout our discussion of in-situ results, we have tended to emphasize the use of only chargeability and time constant for discrimination between different types of mineralization. The reason for this is that the two other parameters in our Cole-Cole complex resistivity model showed relatively minor variation with mineral type. As illustrated by the histograms in Figure 23, the mean value for the frequency dependence c was near 0.25 for all our in-situ spectral measurements. This value correlates well with the results of earlier laboratory studies by Madden and Cantwell (1967). The only type of mineralization for which the frequency-dependence is perhaps significantly less than 0.25 is dry porphyry

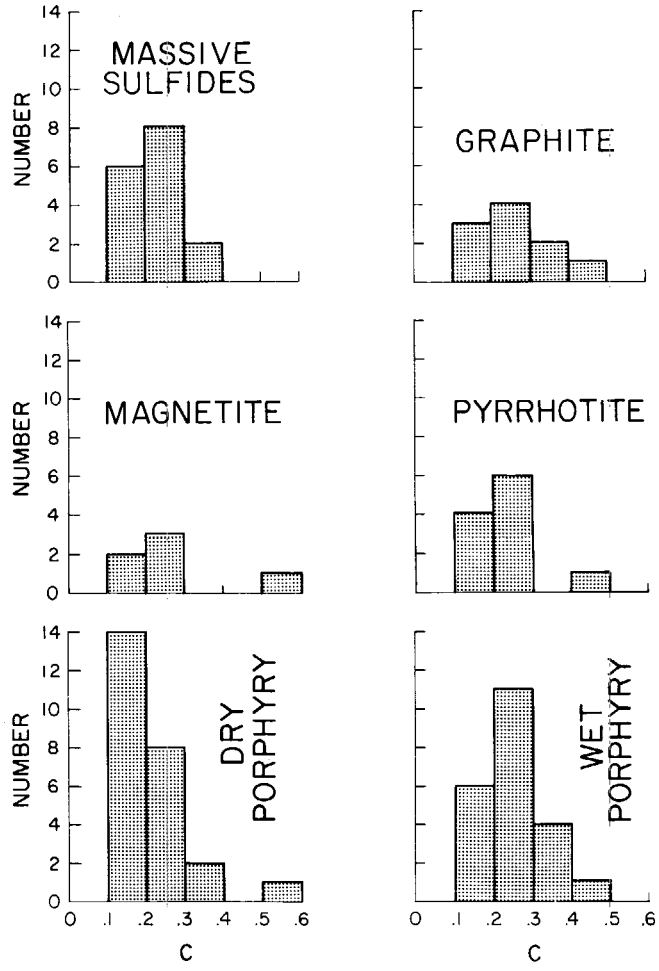

FIG. 23. Histograms showing the variation in frequency dependence c for the various types of mineralization. The mean value of c is 0.25 for each different type of mineralization.

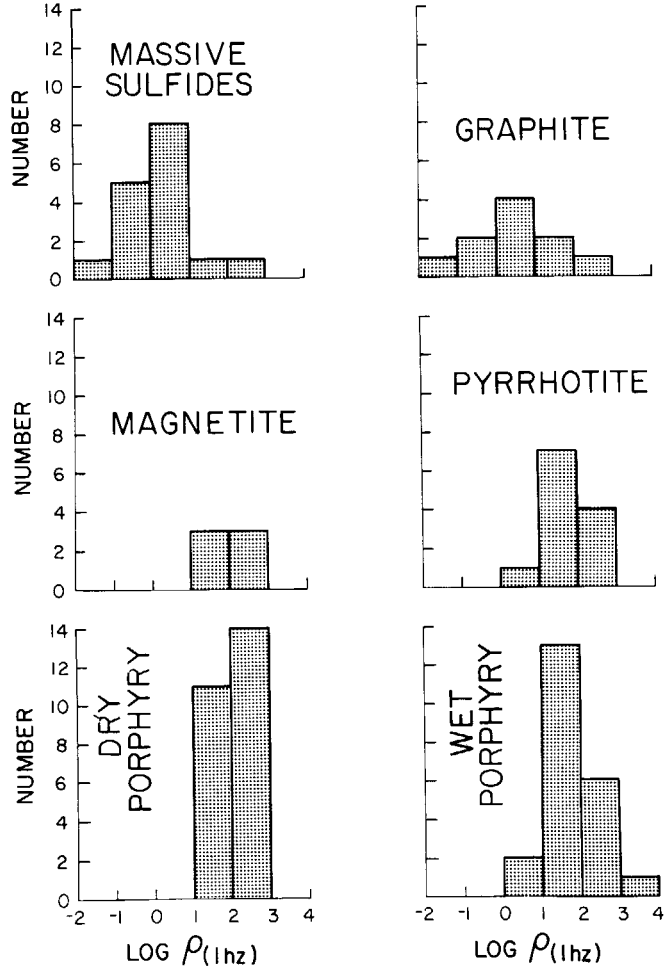

FIG. 24. Histograms showing the variation in resistivity at 1.0 Hz for the various types of mineralization.

mineralization. For this type of mineral occurrence, the phase peaks are often quite broad and the frequency dependence is correspondingly small, as found by Van Voorhis et al (1973).

Similar histograms are shown in Figure 24 for the log of the resistivity at 1 Hz. We used these resistivity values since the values were more accurately known than those of the dc resistivity R_0. As can be seen from the figure, the resistivities we obtained over graphite are very similar to those obtained over massive sulfides. Mean values for both types of mineralization are near 3.0 Ω-m. A slight difference is evident between the resistivities of wet and dry porphyry mineralization. This correlated with the general observation that resistivities over disseminated mineralization in the core of a porphyry are higher than those obtained over the surrounding pyrite halo. Our third set of histograms, contrasting the resistivities of pyrrhotite and magnetite, are perhaps a little misleading. Although the values for both types of mineralization are similar, we mentioned that we were forced to place part of our electrode array on host rock at Sudbury in order to obtain voltages large enough to measure. Also, at Cavendish none of the pyrrhotite mineralization was exposed. As a result, it was necessary to average the effect of overburden with the mineralization. Both actions caused the apparent resistivities reported for pyrrhotite to be larger than the true resistivities.

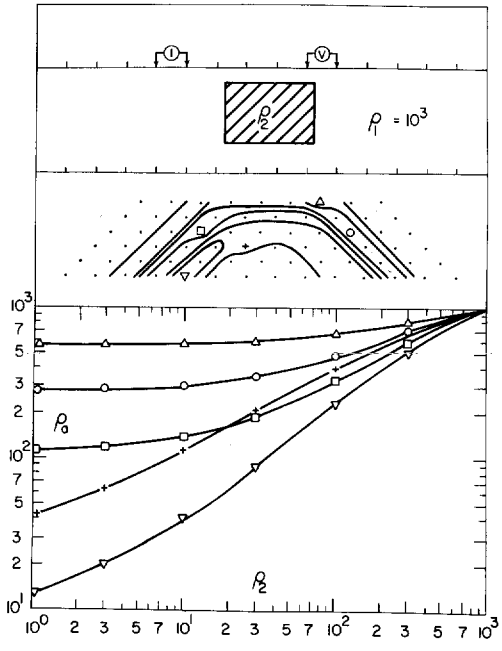

FIG. 25. Plots of apparent resistivity versus the true resistivity of a two-dimensional body. The symbols in the pseudosection indicate the positions of the different apparent resistivity values shown in the plots.

CORRECTIONS FOR FINITE BODIES

Our difficulties in obtaining the true versus apparent resistivity for pyrrhotite rather naturally lead to the question of true versus apparent for the other spectral parameters: chargeability, time constant, and frequency-dependence. Most of our measurements on the other types of mineralization approximated homogeneous earth conditions, but of course, such conditions are rarely achieved in the field. Thus in order to make use of spectral IP measurements in practical exploration problems, we must understand the variations in spectra that can arise from finite bodies.

It turns out that these variations can be predicted accurately from the knowledge of only one additional parameter, which we call here the "dilution factor",

$$B_2 = \frac{\partial \ln \rho_a}{\partial \ln \rho_2}, \tag{6}$$

where ρ_a is the apparent resistivity and ρ_2 is the resistivity of the polarizable body. This is the same factor which has long been used to obtain the apparent polarizability anomaly (PFE_a) arising from a polarizable body (PFE_2),

$$PFE_a = B_2 \cdot PFE_2, \tag{7}$$

in nonpolarizable host rock (Seigel, 1959).

Figure 25 shows five apparent resistivity data points and the curves describing their variation with the resistivity of the target. The dilution factor B_2 is just the slope of these double logarithmic curves. We note that depending on the particular apparent resistivity data point and the resistivity contrast, the dilution factors range from nearly 1.0 to almost zero.

In Figure 26, we show a plot of complex resistivity amplitude versus frequency for a theoretical IP source having the spectral parameters $R_0 = 1.0$, $m = 0.95$, $\tau = 1.0$, and $c = 0.25$. The normalized apparent amplitude curves which would be measured over this source for particular electrode geometries giving rise to dilution factors $B_2 = 0.5$, $B_2 = 0.25$, and $B_2 = 0.125$ are also shown in the figure. It is evident that a small dilution factor results in an apparent amplitude curve with much gentler slope than that of the true amplitude curve for the body. In fact, the slope of the apparent amplitude curve at

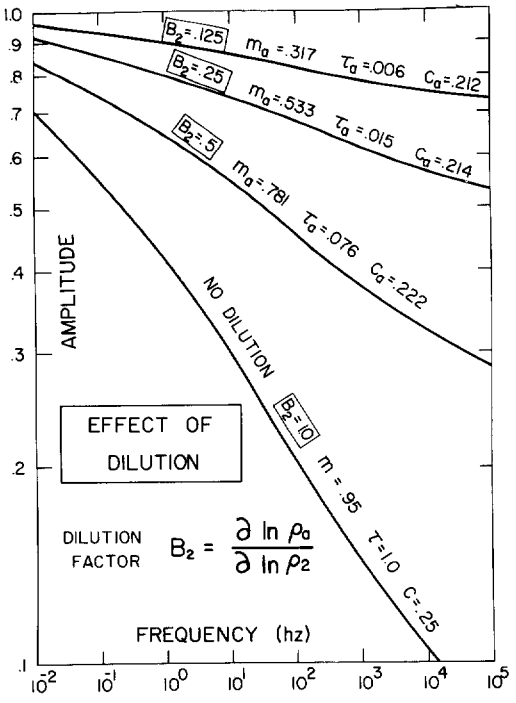

FIG. 26. Amplitude spectra obtained over a polarizable homogeneous earth and apparent amplitude spectra obtained over finite bodies having the same polarizability parameters as that of the homogeneous earth but having differing geometries, which results in differing values of the dilution factor B_2.

any frequency is just B_2 times the slope of the true amplitude curve at that frequency (6). If we assume that B_2 is relatively constant over the resistivity change produced by polarization, an assumption which is implicit in Seigel's original derivation, we can very readily obtain the complete normalized apparent amplitude curve $Z_a(\omega)$ from the actual normalized amplitude curve $Z_a(\omega)$ through the relation,

$$Z_a(\omega) = [Z(\omega)]^{B_2}. \qquad (8)$$

By normalization here, we mean that the amplitude value at zero frequency is equal to 1.0. The actual apparent amplitude at dc is, of course, already known from the apparent resistivity pseudosection.

Since we are already familiar with apparent resistivity data arising from a finite ore body, the apparent value of the parameter R_0 presents no mystery. What does interest us though, are the apparent values for the other three spectral parameters. Unfortunately, there is no easy analytical formula relating the apparent parameters m_a, τ_a, and c_a in terms of the true parameters and the dilution factor B_2. In fact, the apparent amplitude spectra no longer exactly correspond to a Cole-Cole model. The fit is very close, however, and listed in Figure 26 are the apparent parameter values obtained from inversion of the apparent amplitude spectra.

We note that the apparent frequency dependence c_a shows relatively minor variation with dilution factor. The values .222, .214, and .212 are all reasonably close to the true frequency dependence $c = 0.25$. The apparent chargeability and apparent time constant, however, show significant variation with B_2. In order to demonstrate this variation more clearly, we have constructed the nomogram shown in Figure 27. For all the results presented in the nomogram, the true frequency dependence was 0.25 and the true time constant was 1.0. Each solid line corresponds to a polarizable body with a specific chargeability. It is evident that as the dilution factor decreases from 1.0 (no dilution) to 0.125, the apparent chargeability and apparent time constant also both decrease. The decrease in apparent time constant is three orders of magnitude for highly polarizable bodies ($m = 0.98$), but is relatively minor for bodies with lower polarizability ($m = .15$ to $.55$).

Since the nomogram has a logarithmic horizontal scale, it is evident that selection of a true time constant other than $\tau = 1.0$ would result in only shifting the complete set of curves to the right or left. The curves are thus very useful; they describe the trajectory in chargeability-time constant space for virtually any polarizable body having the frequency dependence $c = 0.25$, which was the mean frequency dependence for all our in-situ spectral data.

If we now return to Figure 22, we can understand more readily the low apparent chargeability (0.6) and small apparent time constant (10^{-3} sec) measured over the Seneca deposit in British Columbia. Since we were separated from the mineralization by a layer of debris, the true chargeability of the sulfides was obviously higher, perhaps near 0.85. If this value were known to be the true chargeability of the sulfides, we could superimpose the nomogram and immediately determine that the true time constant of the sulfides is roughly one decade higher and that the dilution factor for the measurement was about 0.5. It would then be possible to use this information about B_2 to help determine the true resistivity section for the earth. Alternatively, if we have no information on the true chargeability of the body, but instead have relatively complete apparent resistivity data, we can invert the data (Pelton et al, 1976) to determine the approximate resistivity section and thus the dilu-

tion factor. From knowledge of m_a, τ_a, and B_2, we can then determine from the nomogram the true chargeability and true time constant for the body.

Using these principles, it is possible to correct the data for pyrrhotite presented in Figure 19 and thereby determine the true spectral parameters for the mineralization. Since the dilution factor for some of the measurements at Sudbury and Cavendish was at least as small as 0.5, the data corresponding to low apparent chargeabilities have probably been shifted significantly down and to the left in chargeability-time constant space. Those data corresponding to apparent chargeabilities in the range 0.3 to 0.5 probably reflect true chargeabilities of at least 0.6 and true time constants at least half a decade larger than the measured apparent values.

REMOVAL OF INDUCTIVE COUPLING

Our in-situ measurements, in addition to presenting encouragement for possible mineral discrimination based on texture, also provide information of value on the removal of inductive electromagnetic coupling effects from IP data. Numerical calculations of EM coupling phase angles due to a dipole-dipole array on a homogeneous earth (Millet, 1967) and on a layered earth (Hohmann, 1973) yield low-frequency asymptotes having slopes very close to 1.0 on a double logarithmic plot. Although the phase angle curves are typically asymmetric, as illustrated in Figure 28, the low frequency half of the phase angle coupling curve can be accurately approximated by a Cole-Cole model with frequency dependence typically between .95 and 1.0.

These values are very much higher than the 0.25 mean value for the frequency dependence of polarizable mineralization obtained from our in-situ studies. It thus appears quite reasonable to use these differences in frequency dependence in attempting to discriminate between the IP effects arising from coupling.

Figure 29 shows phase angle data obtained with our high-frequency in-situ equipment where we deliberately created inductive coupling by increasing our electrode interval to 30 m. Since the test was conducted over alluvium, the true IP response of the ground was very small. As illustrated in the figure, we were able to fit, quite accurately, the field data with two Cole-Cole dispersions: one having a frequency dependence near 1.0, presumably corresponding to the coupling, and the other with a frequency dependence of 0.25, presumably corresponding to polarizable clays in the alluvium. Since we

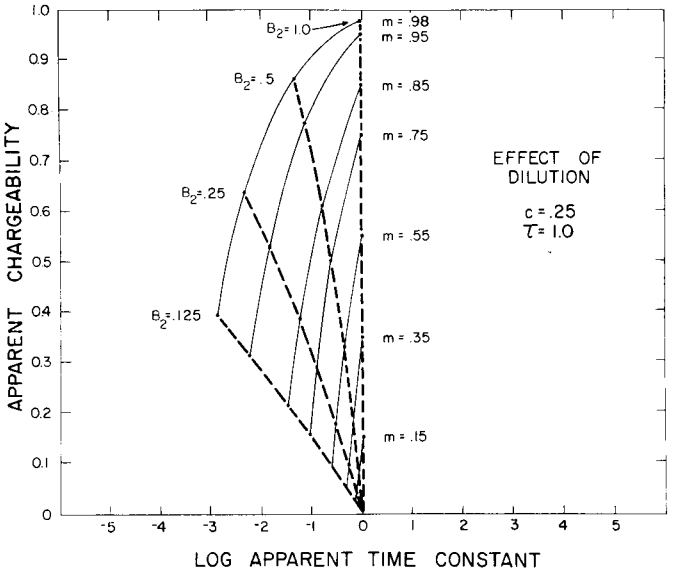

FIG. 27. Nomogram showing the change in apparent chargeability and apparent time constant caused by varying the dilution factor B_2. The dashed lines are lines of constant B_2. The solid lines show how the observed chargeability and observed time constant change as a finite body becomes more deeply buried (i.e., the dilution factor changes from 1.0 to 0.125).

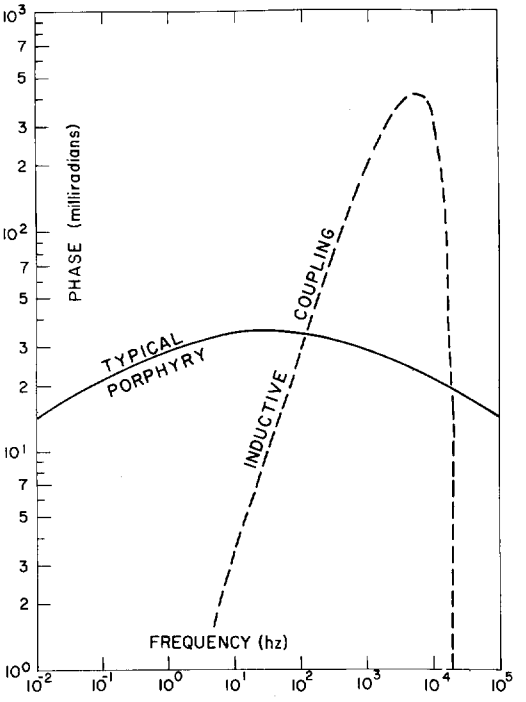

FIG. 28. Phage angle spectra for typical porphyry copper mineralization (solid line) and for inductive electromagnetic coupling due to a homogeneous earth (dashed line).

took very little low-frequency data, the determination of the chargeability and time constant for the clays was very inaccurate; thus the "coupling removed" curve, which we constructed from these poorly determined parameters, is only approximate. The time constant for the high-frequency disperson, on the other hand, was well-determined. We were able to use this time constant to obtain an estimate for the homogeneous earth resistivity, since the inductive coupling is a known function of the resistivity, frequency, and electrode spacing. The resistivity thus obtained was in reasonably good agreement (within 30 percent) with the measured apparent resistivity value of 178 Ω-m.

In order to test the coupling removal program on slightly more realistic data, we inverted field results (Figure 30) provided by Wynn (1975). Since the data adequately covered the lower frequency range down to 0.1 Hz, we obtained good determinations for both the chargeability and time constant of the low-frequency relaxation as well as the time constant for the inductive coupling. Using the well-determined parameters for the low-frequency IP dispersion, we were able to construct with reasonable confidence the coupling removed curve shown in the figure.

SUMMARY AND CONCLUSIONS

Our in-situ measurements tend to confirm suggestions from earlier laboratory studies (Madden and Cantwell, 1967; Pelton et al, 1972) that IP spectra generally conform to the Cole-Cole relaxation model. The frequency dependence for this model ranges between 0.1 and 0.6, with a mean value near 0.25. However, this parameter is relatively independent of mineral type. Two other spectral parameters, the chargeability and the time constant, show much wider variation between different types of mineralization and, consequently, hold greater promise as useful tools in possible mineral discrimination.

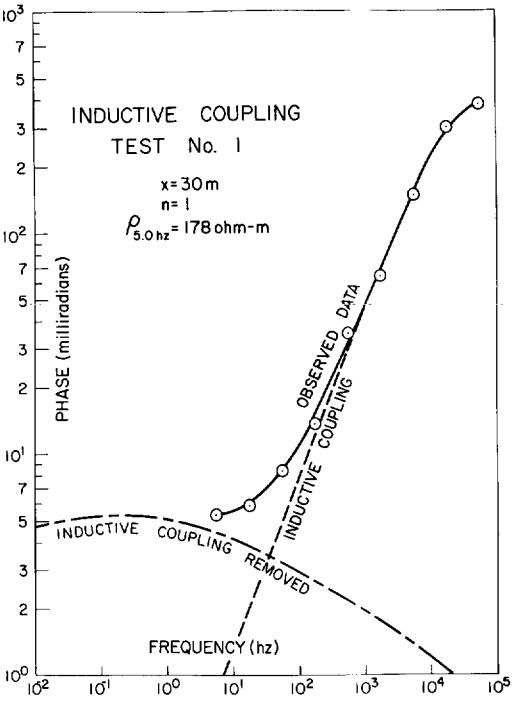

FIG. 29. Phase angle IP data (circles) obtained over alluvium. The data are almost completely dominated by inductive coupling effects. After using ridge regression inversion to automatically fit two Cole-Cole dispersions (solid line) to the data, the parameters obtained for each dispersion were used to construct the dispersion due to coupling effects alone (dashes) and the dispersion due to IP effects alone (dots and dashes). The IP dispersion was presumed to have a frequency dependence equal to 0.25, whereas the frequency dependence for the inductive coupling was determined by the inversion to be near 1.0.

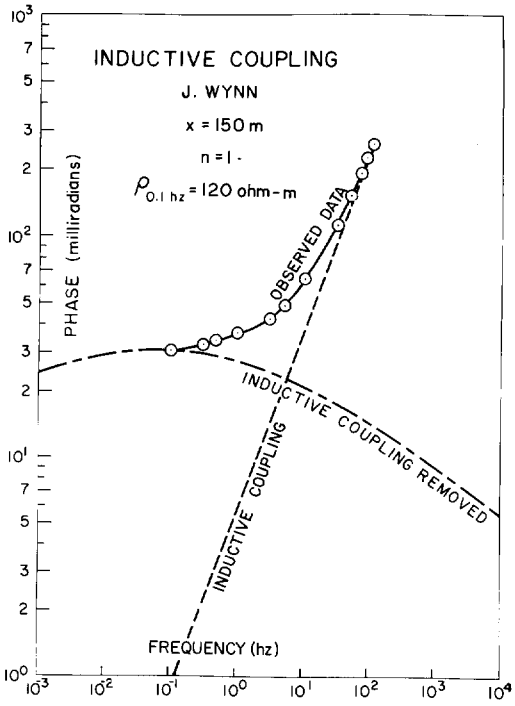

FIG. 30. Phase angle IP data (circles) provided by Wynn (1975). Beyond 10 Hz the data are dominated by inductive coupling effects. The same procedure outlined in Figure 29 was used to remove the inductive coupling effects from the IP data.

It appears that rudimentary discrimination between graphite and massive sulfides might possibly be accomplished by simply observing if the phase angle increases from 0.1 to 1.0 Hz (massive sulfides) or decreases (graphite). Alternatively, if data over a broader frequency range are available, the results may be inverted to provide estimates for the chargeability and time constant of the mineralization. Although the chargeabilities for massive sulfides and graphite are similar, there appears to be a difference of several orders of magnitude in the time constant—from approximately 10^{-1} sec for massive sulfides to 10^{+3} sec for graphite.

Similar differences have been found in the spectra of typical pyrrhotite and magnetic mineralization and in the spectra of wet as opposed to dry porphyry mineralization. All of these differences in IP spectra appear to be caused mainly by mineral texture. Laboratory studies of the interface impedance and studies of variable grain size and sulfide concentration in artificial rocks, as well as our in-situ results, all point toward the conclusion.

A difficulty in the interpretation of multifrequency IP data arises from the apparent spectra observed over targets of finite size. In order to obtain the true chargeability and true time constant of the polarizable material, it is necessary to know the dilution factor,

$$B_2 = \frac{\partial \ln \rho_a}{\partial \ln \rho_2}.$$

This factor may be derived from knowledge of the resistivity section which may, in turn, be obtained from inversion of the apparent resistivity data. Or, alternatively, if the true chargeability is known or presumed known, it is possible to determine the dilution factor from the difference between the true chargeability and the apparent chargeability. This information can then be used in the interpretation of the apparent resistivity data.

A further outcome from our in-situ studies has been the conclusion that the frequency dependence of IP effects due mineralization is much lower than the frequency dependence of the effects due to inductive electromagnetic coupling. As a result, inductive coupling effects may be automatically removed from spectral IP data by inversion.

ACKNOWLEDGMENTS

This research has been supported by Grant GA-31571 provided by the National Science Foundation and by equipment and travel funds provided by Kennecott Exploration, Inc. and Cominco Ltd. We are also deeply grateful to a total of 21 Canadian and U.S. mineral companies, and also the Geological Survey of Canada, which were very helpful in providing assistance in site selection and access to the various open pit mines as well as, in some instances, actual help with the field measurements and field expenses. Finally, one of us (W.P.) would like to express sincere appreciation to James D. Klein for his kind assistance and unfailing good humor throughout two summers of field work.

REFERENCES

Cole, K. S., and Cole, R. H., 1941, Dispersion and absorption in dielectrics; J. Chem. Phys., v. 9, p. 341.

Fraser, D. C., Keevil, N. B., Jr., and Ward, S. H., 1964, Conductivity spectra of rocks from the Craigmont ore environment: Geophysics, v. 29, p. 832–847.

Grisseman, C., 1971, Examination of the frequency-dependent conductivity of ore-containing rock on artificial models: Scientific rep. no. 2, Electronics Laboratory, University of Innsbruck, Austria.

Hallof, P. G., 1965, The proper choice of frequencies for induced polarization measurements: Presented at the 35th Annual International SEG Meeting, November 16 in Dallas.

——— 1974, The IP phase measurement and inductive coupling: Geophysics, v. 39, p. 650–665.
Hohmann, G. W., 1973, Electromagnetic coupling between grounded wires at the surface of a two-layer earth: Geophysics, v. 38, p. 854–863.
Katsube, T. J., 1976, Complex resistivity and new IP parameters: Presented at the 46th Annual International SEG Meeting, October 26 in Houston.
Klein, J. D., and Pelton, W. H., 1976, A laboratory investigation of the complex impedance of mineral-electrolyte interfaces: Presented at the 46th Annual International SEG Meeting, October 26 in Houston.
Madden, T. R., and Cantwell, T., 1967, Induced polarization, a review, *in* Mining geophysics, Vol. 2: Tulsa, SEG, p. 373–400.
Millet, F. B., 1967, Electromagnetic coupling of colinear dipoles on a uniform half space, *in* Mining geophysics, Vol. 2: Tulsa, SEG, p. 401–419.
Pelton, W. H., Rijo, L., and Swift, C. M. Jr., 1976, Inversion of two-dimensional induced polarization and resistivity data: Presented at the 46th Annual International SEG Meeting, October 26 in Houston.
Pelton, W. H., Smith, B. D., and Sill, W. R., 1974, Inversion of complex resistivity and dielectric data: Presented at the 44th Annual International SEG Meeting, November 12 in Dallas.
Pelton, W. H., and Smith, P. K., 1976, Mapping porphyry copper deposits in the Philippines with IP: Geophysics, v. 41, p. 106–122.
Pelton, W. H., Smith, R. J., and Hallof, P. G., 1972, Parameters to describe second-order IP effects in the frequency domain: Toronto, McPhar Geophysics, Ltd.
Seigel, H. O., 1959, Mathematical formulation and type curves for induced polarization: Geophysics, v. 24, p. 547–565.
Sill, W. R., and DeWitt, G., 1976, Parametric studies of IP spectra: Presented at the 46th Annual International SEG Meeting, October 26 in Houston.
Van Voorhis, G. D., Nelson, P. H., and Drake, T. L., 1973, Complex resistivity spectra of porphyry copper mineralization: Geophysics, v. 38, no. 1, p. 49–60.
Wynn, J. C., and Zonge, K. L., 1975, EM coupling, its intrinsic value, its removal and the cultural coupling problem: Geophysics, v. 40, p. 831–851.
Zonge, K. L., and Wynn, J. C., 1975, Recent advances and applications in complex resistivity measurements: Geophysics, v. 40, p. 851–864.